




The polarization quaternion and its applications: a joint representation of the Q/U Stokes parameters and E/B mode polarizations

Hao Liu ^{1,*}, James Creswell,^{2,†} Chao-Wei Tsai ^{3,‡} and Pavel Naselsky ^{4,§}

¹*School of Physics and optoelectronics engineering, Anhui University, 111 Jiulong Road, Hefei, Anhui, China 230601.*

²*Arnold Sommerfeld Center for Theoretical Physics, Ludwig Maximilian University of Munich, Theresienstr. 37, 80333 Munich, Germany.*

³*National Astronomical Observatories, Chinese Academy of Sciences,*

20A Datun Road, Chaoyang District, Beijing, 100012, People's Republic of China.

⁴*The Niels Bohr Institute, Blegdamsvej 17, DK-2100 Copenhagen, Denmark.*

In this work, we point out that the Q/U Stokes parameters and E/B mode polarizations are the four components of a unique quaternion, which describes at the same time the directions and the parity states of spherical linear polarizations. We then point out that, with this polarization quaternion, the mathematical form of all Q/U and E/B transforms are greatly simplified, to an extent that requires only one quaternion multiplication for each transform. A preliminary application of the polarization quaternion is shown as an example to detect peculiar pixel domain patterns within the E- and B-families, which are the former and latter halves of the polarization quaternion.

CONTENTS

I. Introduction	2
II. Review of the basis	2
III. Quaternion representation of the E and B families	4
A. The pixel-to-harmonic domain transform	4
B. The pixel-to-pixel domain transform	6
C. Transform the polarization quaternion to the harmonic domain and back	6
D. Alternative forms	6
1. Different choices of the quaternion conjugates	6
2. Different definitions of the basic quaternions	7
IV. The eigen-problem of a quaternionic system and the parity space	8
A. The eigen-problem of a quaternionic system	8
B. From real space to parity space	8
V. Example of application	9
A. Morphology of the E- and B-families	9
B. Toy model of the mechanism of B-family emissions	12
VI. Discussion	15
Acknowledgments	15
A. The system of quaternion multiplication	16
1. The system of quaternion conjugates	16
2. The system of quaternion matrix multiplication	17
B. Quick reference of the E and B family decomposition with quaternions	18
References	19

* ustc_liuhao@163.com

† creswelljames@gmail.com

‡ cwtsai@nao.cas.cn

§ naselsky@nbi.dk

I. INTRODUCTION

In modern cosmology, one of the working hypotheses holds that the large-scale structure of matter is related to the evolution of quantum fluctuations during the inflationary expansion of the Universe. The cosmic microwave background and its anisotropy and polarization are the strongest observational evidences of this theory. The B-mode of the primordial CMB polarization encodes the tensor to scalar ratio r , which measures the power of gravitational waves in the early Universe that are related to the inflationary potential. Planck observations limit r to about $r \leq 0.036 - 0.1$ [1–5]. Unfortunately, the theoretical predictions of the r -parameter are model-dependent and range from 10^{-2} to 10^{-4} . In the next decade, there will be new efforts to study the CMB polarization in order to improve constraints on cosmological parameters and the physics of inflation. The next generation of CMB experiments include LiteBIRD [6], CMB-S4 [7], the Simons Observatory [8], POLARBEAR [9], and AliCPT [10]. These experiments are targeting a sensitivity of $r = 0.001$. However, the lesson after BICEP2 is that measuring only the power spectrum of the B-mode polarization, which in the simplest theoretical simulation is zero in the absence of cosmological gravitational waves (GW), is insufficient.

Additionally to the power spectrum estimation, special attention should be paid to the study of the statistical properties of the B-mode sky map in order to isolate potential non-Gaussianities indicating its contamination by foreground remnants and systematic effects. The obvious importance of this problem for understanding the physics of inflation and GWs requires the development of methods complementary to the standard decomposition of the Q/U Stokes parameters into E/B components. If we are sure that in the absence of cosmological GWs we have zero B-mode, but the measured B-mode is non-zero and Gaussian, this signal would be an important indicator of the properties of inflation. But already the experience of Planck shows that at $r \sim 0.05 - 0.10$ the B-mode polarization is different from zero, and is associated with non-cosmological (and non-Gaussian) signals. Here one should also add the effect of lensing of the primary E-mode, leading to the appearance of a nonzero B-mode even in the absence of GWs.

Thus, in addition to the standard transition $(Q, U) \rightarrow (E, B)$, where the Stokes parameters (Q, U) are treated as components of a pseudo-vector and convolved into a combination of scalar E and pseudoscalar B, it is important to analyze also the possibility of transforming Q/U into two pseudo-vectors (Q_E, U_E) and (Q_B, U_B) called the E- and B-families [11], where the B-family (Q_B, U_B) is still zero in the absence of GWs and lensing. Among other interesting properties, this conception of the E/B decomposition leads to useful approaches in polarized foreground analysis [11, 12].

To achieve this goal, we will in this paper augment the previous work [11] and exploit the concept of quaternion decomposition of the Stokes parameters into (Q_E, U_E) and (Q_B, U_B) , which leads to two pairs of maps with morphology different from the morphology of the scalar E and B maps.

The quaternion concept was introduced by the Irish mathematician William Rowan Hamilton in 1843, and the German mathematician Frobenius in 1877 proved that every finite-dimensional associative division algebra over the real numbers is isomorphic to one of the three: real numbers, complex numbers and the quaternions. Here we present implementation of that concept for the CMB polarization from the recent Planck data release. The idea is to represent the polarization data as a quaternion with (Q_E, U_E) and (Q_B, U_B) in separate quaternionic components. Then the E and B modes, in either harmonic ($a_{E/B, \ell m}$) or real-space ($P_{E/B}$) representations, are related by convolution with an appropriate kernel. Again exploiting the dimensions of the quaternion to combine the E and B modes into a single mathematic object, the equations can be written compactly, and new mathematical properties of the E/B transform are revealed. Furthermore, we also consider generalizations such as the quaternionic spin eigensystem for arbitrary spins and the general relation between the real space maps and the parity space representation.

The outline of the paper is the follows: In Section II the formalism of the Stokes-space EB family decomposition is reviewed, and Section III presents the new theory of the polarization quaternion. In Section IV the quaternionic eigenproblem of a spin system is discussed, and Section V is devoted to application of the EB-families to foreground analysis, focusing especially on the Planck 30 GHz and 353 GHz frequency maps, in comparison with other astrophysical datasets. The results reveal local features associated with B-mode emission. Lastly a brief discussion is given in Section VI.

II. REVIEW OF THE BASIS

We start from the well known forward-backward spin-2 spherical harmonics transforms of the Stokes parameter:

$$\begin{aligned}
 a_{\pm 2, \ell m} &= \int (Q \pm U i) [{}_2 Y_{\ell m}^*] d\mathbf{n} \\
 Q \pm U i &= \sum_{\ell m} a_{\pm 2, \ell m} [{}_{\pm 2} Y_{\ell m}],
 \end{aligned}
 \tag{1}$$

note that $Q = Q(\mathbf{n})$, $U = U(\mathbf{n})$ and ${}_{\pm 2}Y_{\ell m} = {}_{\pm 2}Y_{\ell m}(\mathbf{n})$ are all functions of the unit pointing vector \mathbf{n} , which is omitted in the above equation for convenience. The E- and B-mode harmonic coefficients are defined as ¹:

$$\begin{aligned} a_{E,\ell m} &= \frac{a_{2,\ell m} + a_{-2,\ell m}}{2} \\ a_{B,\ell m} \mathbf{i} &= \frac{a_{2,\ell m} - a_{-2,\ell m}}{2}. \end{aligned} \quad (2)$$

From eq. (1) we get

$$\begin{aligned} Q &= \frac{1}{2} \left(\sum_{\ell m} a_{2,\ell m} [{}_{2}Y_{\ell m}] + \sum_{\ell m} a_{-2,\ell m} [{}_{-2}Y_{\ell m}] \right), \\ U \mathbf{i} &= \frac{1}{2} \left(\sum_{\ell m} a_{2,\ell m} [{}_{2}Y_{\ell m}] - \sum_{\ell m} a_{-2,\ell m} [{}_{-2}Y_{\ell m}] \right), \end{aligned} \quad (3)$$

and by assuming $a_{E,\ell m} = 0$ and $a_{B,\ell m} = 0$ respectively, we get

$$\begin{cases} a_{B,\ell m} = 0 \implies a_{2,\ell m} = a_{-2,\ell m} = a_{E,\ell m} \\ a_{E,\ell m} = 0 \implies a_{2,\ell m} = -a_{-2,\ell m} = a_{B,\ell m} \mathbf{i} \end{cases} \quad (4)$$

Then we define two functions with even and odd parities respectively:

$$F_{+,\ell m} = \frac{1}{2} ({}_{2}Y_{\ell m} + {}_{-2}Y_{\ell m}) \quad F_{-,\ell m} = \frac{1}{2} ({}_{2}Y_{\ell m} - {}_{-2}Y_{\ell m}), \quad (5)$$

which gives

$$\begin{aligned} a_{B,\ell m} = 0 &\implies \begin{cases} Q_E = \sum_{\ell m} a_{E,\ell m} F_{+,\ell m} \\ U_E \mathbf{i} = \sum_{\ell m} a_{E,\ell m} F_{-,\ell m} \end{cases} \\ a_{E,\ell m} = 0 &\implies \begin{cases} Q_B = \sum_{\ell m} (a_{B,\ell m} \mathbf{i}) F_{-,\ell m} \\ U_B \mathbf{i} = \sum_{\ell m} (a_{B,\ell m} \mathbf{i}) F_{+,\ell m} \end{cases}. \end{aligned} \quad (6)$$

Combining eq. (1) and eq. (5) gives

$$\begin{aligned} a_{E,\ell m} &= \frac{a_{2,\ell m} + a_{-2,\ell m}}{2} = \frac{1}{2} \int \{ (Q + U \mathbf{i}) [{}_{2}Y_{\ell m}^*] + (Q - U \mathbf{i}) [{}_{-2}Y_{\ell m}^*] \} d\mathbf{n} \\ &= \int (Q F_{+,\ell m}^* + (U \mathbf{i}) F_{-,\ell m}^*) d\mathbf{n} \\ a_{B,\ell m} \mathbf{i} &= \frac{a_{2,\ell m} - a_{-2,\ell m}}{2} = \frac{1}{2} \int \{ (Q + U \mathbf{i}) [{}_{2}Y_{\ell m}^*] - (Q - U \mathbf{i}) [{}_{-2}Y_{\ell m}^*] \} d\mathbf{n} \\ &= \int (Q F_{-,\ell m}^* + (U \mathbf{i}) F_{+,\ell m}^*) d\mathbf{n}; \end{aligned} \quad (7)$$

Thus, we have

$$\begin{aligned} Q_E(\mathbf{n}) &= \sum_{\ell m} a_{E,\ell m} F_{+,\ell m}(\mathbf{n}) = \\ &= \int d\mathbf{n}' \left\{ Q(\mathbf{n}') \sum_{\ell m} [F_{+,\ell m}(\mathbf{n}) F_{+,\ell m}^*(\mathbf{n}')] + U(\mathbf{n}') \mathbf{i} \sum_{\ell m} [F_{+,\ell m}(\mathbf{n}) F_{-,\ell m}^*(\mathbf{n}')] \right\}. \end{aligned} \quad (8)$$

¹ Note that the definition here is different to the definition in [13] by factor -1 for both the E and B mode coefficients. The reason is that we choose to attach \mathbf{i} to U and $a_{B,\ell m}$ as $U \mathbf{i}$ and $a_{B,\ell m} \mathbf{i}$ to simplify the equations (which is also important for the quaternion form to be presented later). For the same reason, the definition in eq. (5) is also different to our previous work [11] by a constant factor.

Use eq. (7) of [14] to compute the $F_+F_+^*$ and $F_+F_-^*$ terms, we get

$$\begin{aligned} \sum_{\ell m} F_{+, \ell m}(\mathbf{n}) F_{+, \ell m}^*(\mathbf{n}') &= \frac{1}{4} \sum_{\ell} ({}_2Y_{\ell, -2} + {}_2Y_{\ell, 2} + {}_{-2}Y_{\ell, -2} + {}_{-2}Y_{\ell, 2})(\beta, \alpha) \\ &= \sum_{\ell} \operatorname{Re} \left(\sqrt{\frac{2\ell+1}{4\pi}} \frac{{}_2Y_{\ell, -2}(\beta, \alpha) + {}_2Y_{\ell, 2}(\beta, \alpha)}{2} \right) \\ \sum_{\ell m} F_{+, \ell m}(\mathbf{n}) F_{-, \ell m}^*(\mathbf{n}') &= \frac{1}{4} \sum_{\ell} ({}_2Y_{\ell, -2} - {}_2Y_{\ell, 2} + {}_{-2}Y_{\ell, -2} - {}_{-2}Y_{\ell, 2})(\beta, \alpha) \\ &= \sum_{\ell} \mathbf{i} \operatorname{Im} \left(\sqrt{\frac{2\ell+1}{4\pi}} \frac{{}_2Y_{\ell, -2}(\beta, \alpha) - {}_2Y_{\ell, 2}(\beta, \alpha)}{2} \right), \end{aligned} \quad (9)$$

where (β, α) is the Euler angles of rotation from \mathbf{n} to \mathbf{n}' . Continue with the other two combinations gives

$$\begin{aligned} \sum_{\ell m} F_{+, \ell m}(\mathbf{n}) F_{+, \ell m}^*(\mathbf{n}') &= \operatorname{Re}(\mathcal{F}_+); \quad \sum_{\ell m} F_{+, \ell m}(\mathbf{n}) F_{-, \ell m}^*(\mathbf{n}') = \mathbf{i} \operatorname{Im}(\mathcal{F}_-) \\ \sum_{\ell m} F_{-, \ell m}(\mathbf{n}) F_{-, \ell m}^*(\mathbf{n}') &= \operatorname{Re}(\mathcal{F}_-); \quad \sum_{\ell m} F_{-, \ell m}(\mathbf{n}) F_{+, \ell m}^*(\mathbf{n}') = \mathbf{i} \operatorname{Im}(\mathcal{F}_+) \end{aligned} \quad (10)$$

where \mathcal{F}_{\pm} are defined as

$$\begin{aligned} \mathcal{F}_+(\mathbf{n}, \mathbf{n}') &= \sum_{\ell} \sqrt{\frac{2\ell+1}{4\pi}} \frac{{}_2Y_{\ell, -2}(\beta, \alpha) + {}_2Y_{\ell, 2}(\beta, \alpha)}{2} \\ \mathcal{F}_-(\mathbf{n}, \mathbf{n}') &= \sum_{\ell} \sqrt{\frac{2\ell+1}{4\pi}} \frac{{}_2Y_{\ell, -2}(\beta, \alpha) - {}_2Y_{\ell, 2}(\beta, \alpha)}{2}. \end{aligned} \quad (11)$$

Substitute the above equation back to eq. (8) gives

$$Q_E(\mathbf{n}) = \int (\operatorname{Re}[\mathcal{F}_+(\mathbf{n}, \mathbf{n}')] Q(\mathbf{n}') - \operatorname{Im}[\mathcal{F}_-(\mathbf{n}, \mathbf{n}')] U(\mathbf{n}')) d\mathbf{n}'. \quad (12)$$

Continue with U_E, Q_B, U_B and with similar processes we get

$$\begin{aligned} \begin{pmatrix} Q_E \\ U_E \end{pmatrix} &= \int \begin{pmatrix} \operatorname{Re}(\mathcal{F}_+) & -\operatorname{Im}(\mathcal{F}_-) \\ \operatorname{Im}(\mathcal{F}_+) & \operatorname{Re}(\mathcal{F}_-) \end{pmatrix} \begin{pmatrix} Q \\ U \end{pmatrix} d\mathbf{n}' \\ \begin{pmatrix} Q_B \\ U_B \end{pmatrix} &= \int \begin{pmatrix} \operatorname{Re}(\mathcal{F}_-) & -\operatorname{Im}(\mathcal{F}_+) \\ \operatorname{Im}(\mathcal{F}_-) & \operatorname{Re}(\mathcal{F}_+) \end{pmatrix} \begin{pmatrix} Q \\ U \end{pmatrix} d\mathbf{n}'. \end{aligned} \quad (13)$$

This equation is equivalent to eq. (2.23) of [11], but is further simplified.

III. QUATERNION REPRESENTATION OF THE E AND B FAMILIES

In this section, we rewrite all EB-decompositions in quaternionic forms. Some necessary introduction of rules and conventions of quaternion conjugate and multiplication can be found in Appendix A, and for reader's convenience, a direct summary of the main results is given in Appendix B.

A. The pixel-to-harmonic domain transform

By definition, each quaternion has two equivalent forms: either consisting of four real numbers or two complex numbers:

$$z_1 + z_2 \mathbf{j} = (a + b\mathbf{i}) + (c + d\mathbf{i})\mathbf{j} = a + b\mathbf{i} + c\mathbf{j} + d\mathbf{k}. \quad (14)$$

Therefore, with the fact that all the following quantities are ordinary complex numbers: $a_E, a_B \mathbf{i}, F_{\pm, \ell m}, \mathcal{F}_{\pm}, P_E = Q_E + U_E \mathbf{i}, P_B = Q_B + U_B \mathbf{i}$; we can define five quaternions straightforwardly²:

$$\begin{aligned}\mathcal{F}_{\ell m} &= F_{+, \ell m} + F_{-, \ell m} \mathbf{j} \\ \mathcal{G} &= \mathcal{F}_+ + \mathcal{F}_- \mathbf{j} \\ \mathcal{D} &= P_E + P_B \mathbf{j} \\ \mathcal{A}_{\ell m} &= a_{E, \ell m} + (a_{B, \ell m} \mathbf{i}) \mathbf{j} = a_{E, \ell m} + a_{B, \ell m} \mathbf{k} \\ \mathcal{P} &= Q + (U \mathbf{i}) \mathbf{j} = Q + U \mathbf{k},\end{aligned}\tag{15}$$

where $\mathcal{F}_{\ell m}$ is the quaternion version of the spin-spherical harmonic function; \mathcal{G} is the pixel domain quaternionic convolution kernel; \mathcal{D} is the pixel domain polarization quaternion that directly contains the EB-families; \mathcal{A} is the harmonic domain counterpart of \mathcal{D} and is a simple combination of the E- and B-mode harmonic coefficient; and \mathcal{P} is a reduced form of \mathcal{D} that contains only the pixel domain Q and U Stokes parameters.

With these definitions, the complete forward EB-transform (pixel domain to harmonic domain) is given by a simple quaternionic integration:

$$\mathcal{A}_{\ell m} = \int \mathcal{F}_{\ell m}^{*101} \mathcal{P},\tag{16}$$

where $*_{101}$ refers to the type-101 quaternion conjugate (Appendix A 1), which is introduced to match the normal E- and B-mode definitions (more possibilities of conjugate will be introduced below). The above equation gives the E- and B-mode harmonic coefficients at the same time as components of \mathcal{A} . It is also easy to see that the backward transform is (note that we need eq. (A3) to get the following equation):

$$\mathcal{P} = \sum_{\ell m} \mathcal{A}_{\ell m}^{*010} \mathcal{F}_{\ell m} = \sum_{\ell m} \mathcal{F}_{\ell m}^{*010} \mathcal{A}_{\ell m},\tag{17}$$

and the self-consistency of the forward/backward transforms is verified in the following proof (also pay attention to eq. (A3), and note that $\mathcal{P}^{*010} = \mathcal{P}$):

$$\begin{aligned}\mathcal{P} &= \sum_{\ell m} \mathcal{A}_{\ell m}^{*010} \mathcal{F}_{\ell m} = \sum_{\ell m} \left(\int \mathcal{F}_{\ell m}^{*101} \mathcal{P} \right)^{*010} \mathcal{F}_{\ell m} \\ &= \sum_{\ell m} \left(\int \mathcal{P}^{*010} (\mathcal{F}_{\ell m}^{*101})^{*010} \right) \mathcal{F}_{\ell m} = \sum_{\ell m} \left(\int \mathcal{P}^{*010} \mathcal{F}_{\ell m}^{*111} \right) \mathcal{F}_{\ell m} \\ &= \sum_{\ell m} \int \mathcal{P} (\mathcal{F}_{\ell m}^* \mathcal{F}_{\ell m}) \\ &= \int d\mathbf{n}' \mathcal{P}(\mathbf{n}') \sum_{\ell m} \mathcal{F}_{\ell m}^*(\mathbf{n}') \mathcal{F}_{\ell m}(\mathbf{n}) \\ &= \mathcal{P}.\end{aligned}\tag{18}$$

If we write $\mathcal{F}_{\ell m}$ into a quaternion matrix \mathcal{F} ³, with the columns being the value of $\mathcal{F}_{\ell m}$ at the spherical directions \mathbf{n} (preferably sorted in the HEALPix [15] ring ordering) and rows being the value of $\mathcal{F}_{\ell m}$ at combination of ℓ and m , sorted with an ℓ -first dictionary order, and correspondingly convert \mathcal{P} and \mathcal{A} into column vectors of consistent orders, then eqs. (16–17) can be further simplified as

$$\begin{aligned}\mathcal{A} &= \mathcal{F}^{H_{101}} \mathcal{P} \\ \mathcal{P} &= \mathcal{F}^{*010} \mathcal{A},\end{aligned}\tag{19}$$

where H_{101} is analog to the conjugate transpose of matrices, but the conjugate part must be of type-101, and $*_{010}$ means a type-010 conjugate without transposing. This is quite different to a complex matrix because a quaternion matrix has seven conjugates rather than one. The above equations are self-consistent because we can easily prove $\mathcal{F}^{*010} \mathcal{F}^{H_{101}} = \mathbf{I}$, i.e., the \mathcal{F} matrix is unitary.

² Note that we use math calligraphy characters for quaternions, bold letters for matrices and vectors, and follow footnote 1 to attach \mathbf{i} with U and a_B ,

³ For the matrix form \mathcal{F} , we no longer need the subscripts ℓm , because they are now the column indices of the matrix.

B. The pixel-to-pixel domain transform

The pixel-to-pixle domain EB-family decomposition is

$$\mathcal{D} = \int \mathcal{G}(\mathbf{n}, \mathbf{n}') \mathcal{P}(\mathbf{n}') d\mathbf{n}' = \mathcal{G} * \mathcal{P}. \quad (20)$$

Like above, this can be further simplified to a quaternion matrix form as

$$\mathcal{D} = \mathcal{G}\mathcal{P}, \quad (21)$$

where \mathcal{G} is a quaternion matrix with the columns and rows being the values of \mathcal{G} at $(\mathbf{n}, \mathbf{n}')$, respectively. Note that because quaternion multiplication is non-commutative, we must be very careful in changing the order of all quaternion equations, especially the ones in combination with a matrix multiplication. This is further discussed in Appendix A.

C. Transform the polarization quaternion to the harmonic domain and back

It is also easy to prove that we can get \mathcal{D} directly from \mathcal{A} by using only the spin-2 spherical harmonic function:

$$\begin{aligned} \mathcal{D} &= \sum_{\ell m} (F_{+, \ell m} + F_{-, \ell m}) \mathcal{A}_{\ell m} = \sum_{\ell m} {}_2Y_{\ell m} \mathcal{A}_{\ell m} \\ \mathcal{A}_{\ell m} &= \int {}_2Y_{\ell m}^* \mathcal{D}, \end{aligned} \quad (22)$$

Let \mathcal{Y}_2 be a matrix form with the columns being the values of ${}_2Y_{\ell m}(\mathbf{n})$ at various \mathbf{n} , and the rows being its values at different combinations of ℓ and m ; then we get the matrix forms of the above equations:

$$\begin{aligned} \mathcal{D} &= \mathcal{Y}_2 \mathcal{A} \\ \mathcal{A} &= \mathcal{Y}_2^H \mathcal{D}, \end{aligned} \quad (23)$$

where $H \equiv H_{111}$ means to take the full conjugate transpose of the quaternion matrix. Therefore, by using the E and B families, the spherical harmonic transform of polarizations can be done even without a minus-spin spherical harmonics.

D. Alternative forms

Due to quaternion's complexity, the form of transform is not unique. In this section, we discuss the possibilities of various forms of the transform.

1. Different choices of the quaternion conjugates

The forward and backward EB-transforms can actually be expressed using the other types of quaternion conjugates (see Appendix A 1), provided that they are paired correctly. The pairs are type-1/type-6, type-3/type-4, in addition to the type-2/type-5 used above. Depending on the type of conjugation used, the specific representation of a_E and a_B in a quaternion form can vary from \mathcal{A}_4 , but in all cases a_E and a_B are well-defined, and it always corresponds to the same E and B power spectra.

Using type-0 conjugation,

$$a_{E, \ell m}^* - a_{B, \ell m}^* \mathbf{k} = \int \mathcal{F}_{\ell m} (Q - U\mathbf{k}), \quad (24)$$

Using type-3 conjugation (011),

$$a_{E, \ell m}^* + a_{B, \ell m}^* \mathbf{k} = \int \mathcal{F}_{\ell m}^{*011} (Q + U\mathbf{k}), \quad (25)$$

Using type-5 conjugation (101), which was already stated above,

$$a_{E, \ell m} + a_{B, \ell m} \mathbf{k} = \int \mathcal{F}_{\ell m}^{*101} (Q + U\mathbf{k}), \quad (26)$$

Using the type-6 conjugation (110) for the forward transform,

$$a_{E,\ell m} - a_{B,\ell m} \mathbf{k} = \int \mathcal{F}_{\ell m}^{*110} (Q - U \mathbf{k}), \quad (27)$$

The other conjugation types produce uneven conjugates between F_+ and F_- that require slightly different representations. Suppose that

$$a_{E,\ell m} = x_{E,\ell m} + y_{E,\ell m} \mathbf{i},$$

where $x_{E,\ell m}$ and $y_{E,\ell m}$ are both real. Then we define the modified $a_{E,\ell m}$ as

$$\bar{a}_{E,\ell m} = x_{E,\ell m} + (-1)^m y_{E,\ell m} \mathbf{i}. \quad (28)$$

The key is, that this kind of modification does not change the power spectrum:

$$\langle |\bar{a}_{E,\ell m}|^2 \rangle = \langle |a_{E,\ell m}|^2 \rangle. \quad (29)$$

type	output	kernel	input
0	$a_E^* - a_B^* \mathbf{k}$	$\mathcal{F}_{\ell m}$	$Q - U \mathbf{k}$
1	$\bar{a}_E^* + \bar{a}_B^* \mathbf{k}$	$\mathcal{F}_{\ell m}^{*001}$	$Q + U \mathbf{k}$
2	$\bar{a}_E^* - \bar{a}_B^* \mathbf{k}$	$\mathcal{F}_{\ell m}^{*010}$	$Q - U \mathbf{k}$
3	$a_E^* + a_B^* \mathbf{k}$	$\mathcal{F}_{\ell m}^{*011}$	$Q + U \mathbf{k}$
4	$\bar{a}_E - \bar{a}_B \mathbf{k}$	$\mathcal{F}_{\ell m}^{*100}$	$Q - U \mathbf{k}$
5	$a_E + a_B \mathbf{k}$	$\mathcal{F}_{\ell m}^{*101}$	$Q + U \mathbf{k}$
6	$a_E - a_B \mathbf{k}$	$\mathcal{F}_{\ell m}^{*110}$	$Q - U \mathbf{k}$
7	$\bar{a}_E + \bar{a}_B \mathbf{k}$	$\mathcal{F}_{\ell m}^{*111}$	$Q + U \mathbf{k}$

TABLE I. Summary of all forward transform types.

2. Different definitions of the basic quaternions

We also point out that the basic quaternion definitions in eq. (15) are not unique. For example, assume we have an alternative form as follows:

$$\begin{aligned} \mathcal{F}_4 &= F_+ + F_- \mathbf{x} \\ \mathcal{A}_4 &= a_E + a_B \mathbf{y} \\ \mathcal{P}_2 &= Q + U \mathbf{z}, \end{aligned} \quad (30)$$

and we still want eq. (16) to be correct. Then by computing the quaternion multiplication and integration and comparing the results with eq. (7), we get the following constraints for x , y and z :

$$xz = \mathbf{i}, \quad y = z, \quad x = -\mathbf{i}y. \quad (31)$$

There are several possible solutions to these three equations, including:

$$1 : \begin{cases} x = 1 \\ y = z = \mathbf{i} \end{cases} \quad 2 : \begin{cases} x = -1 \\ y = z = -\mathbf{i} \end{cases} \quad 3 : \begin{cases} x = \mathbf{j} \\ y = z = \mathbf{k} \end{cases} \quad 4 : \begin{cases} x = -\mathbf{k} \\ y = z = \mathbf{j}. \end{cases} \quad (32)$$

It is easy to prove that solutions 1 and 2 correspond to the basic spin-2 spherical harmonic transforms (eq. 1), and solutions 3 and 4 give two variations of the same E and B decomposition.

IV. THE EIGEN-PROBLEM OF A QUATERNIONIC SYSTEM AND THE PARITY SPACE

A. The eigen-problem of a quaternionic system

According to eq. (23), if the column vector \mathcal{A} contains only one non-zero element, then the matrix multiplication $\mathcal{Y}_2\mathcal{A}$ is nothing but one column of \mathcal{Y}_2 right-multiplied by this non-zero element (as a single quaternion). A more general case is: if a linear spin system can be diagonalized in the space of spin spherical harmonics, then it can be represented by the following equation:

$$\mathcal{M} = \mathcal{Y}_2 \begin{pmatrix} \mathcal{A}_1 & 0 & 0 & \cdots \\ 0 & \mathcal{A}_2 & 0 & \cdots \\ \cdots & \cdots & \cdots & \cdots \\ 0 & 0 & \cdots & \mathcal{A}_n \end{pmatrix} \mathcal{Y}_2^H, \quad (33)$$

where \mathcal{A}_i represents the i -th quaternionic eigenvalue of the \mathcal{M} -system, and the eigenvectors (eigen-modes) of the linear system are nothing but columns of \mathcal{Y}_2 which, with the quaternion multiplication with \mathcal{A}_i , automatically splits into the odd and even parity states of the spin, as components of the quaternionic eigen-state.

Mathematically, eq. (33) is true if all eigen-modes of the system are represented by the spin-spherical harmonics ${}_s Y_{\ell m}$. Therefore, it is the general form of every measurable system that is based on spins.

Eqs. (23, 33) together indicate that spins and parities are probably the two faces of one thing: only that one is more obvious in the pixel domain, whereas the other is more obvious in the harmonic domain.

B. From real space to parity space

Exploration of the quaternion transforms in section III further reveals a new space called the parity space, which is the dual of the real space. First, with Eq. (19) we obtain

$$\mathcal{A} = \mathcal{F}^{H_{101}} \mathcal{P} = \mathbf{a}_{E,\ell m} + \mathbf{a}_{B,\ell m} \mathbf{k}, \quad (34)$$

which means:

$$\mathcal{Y}_0 \mathcal{A} = \mathbf{E} + \mathbf{Bk}, \quad (35)$$

where \mathcal{Y}_0 is the spin-zero spherical harmonic matrix whose columns consist of the values of $Y_{\ell m}(\mathbf{n}) = {}_0 Y_{\ell m}(\mathbf{n})$ at different directions \mathbf{n} . Therefore, we have the following:

$$(\mathbf{E} + \mathbf{Bk}) = \left[\mathcal{Y}_0 \mathcal{F}^{H_{101}} \right] (\mathbf{Q} + \mathbf{Uk}). \quad (36)$$

Apparently, $(\mathbf{Q} + \mathbf{Uk})$ contains all information of polarization in the real space, whereas $(\mathbf{E} + \mathbf{Bk})$ contains the same amount of information, but in a new space called the parity space. Because for polarization, the transform from the real space to the parity space is done by the spin-0 and spin-2 spherical harmonics, we rewrite the above equation and explicitly show spin- s as subscripts:

$$(\mathbf{E} + \mathbf{Bk})_s = \left[\mathcal{Y}_0 \mathcal{F}_s^{H_{101}} \right] (\mathbf{Q} + \mathbf{Uk})_s, \quad (37)$$

whose eigen-system problem (with focus of derivative operators) is fully compatible with the well known angular momentum operators $\hat{\mathbf{L}}_z$ and $\hat{\mathbf{L}}^{(2)}$:

$$\begin{aligned} \hat{\mathbf{L}}_z(\mathbf{E}_{\ell m}) &= m \mathbf{E}_{\ell m} \\ \hat{\mathbf{L}}^{(2)}(\mathbf{E}_{\ell m}) &= \ell(\ell + 1) \mathbf{E}_{\ell m} \\ \hat{\mathbf{L}}_z(\mathbf{B}_{\ell m} \mathbf{k}) &= m \mathbf{B}_{\ell m} \mathbf{k} \\ \hat{\mathbf{L}}^{(2)}(\mathbf{B}_{\ell m} \mathbf{k}) &= \ell(\ell + 1) \mathbf{B}_{\ell m} \mathbf{k} \end{aligned} \quad (38)$$

For simplicity, we write $\rho_s = (\mathbf{E} + \mathbf{Bk})_s$ for the parity space; and $P_s = (\mathbf{Q} + \mathbf{Uk})_s$ for the real space, then the relationship between the real and parity spaces is nothing but

$$\rho_s = \left[\mathcal{Y}_0 \mathcal{F}_s^{H_{101}} \right] P_s. \quad (39)$$

A special case is $s = 0$, (e.g., temperature anisotropy), which shows $\rho_0 = P_0 = T$, i.e., the real and parity spaces are identical for $s = 0$. This also indicates that both real and parity spaces belong to the pixel domain.

An interesting fact is: although we can measure all four Stokes parameters: I , Q , U and V in the real world, they are actually distributed in two different spaces: I and V are in the parity space; whereas Q and U are in the real space. Therefore, the four Stokes parameters cannot be properly included in one quaternion state. Another fact is: it is possible to transform ρ_s back to P_s using another spin $s' \neq s$, which is related to the possible coupling of two systems with different intrinsic spins, i.e., the parity space is probably a convenient bridge between different spins.

V. EXAMPLE OF APPLICATION

A. Morphology of the E- and B-families

In this section we provide some examples of the application of the E and B families. The primary estimators in use are the polarization intensities of the E and B families, which can be written using the normal complex or quaternion modulus

$$\|P_E\| = \|Q_E + U_E i\| = \sqrt{Q_E^2 + U_E^2} \quad (40)$$

$$\|P_B\| = \|Q_B + U_B i\| = \sqrt{Q_B^2 + U_B^2}, \quad (41)$$

and the corresponding orientation of the Stokes fields. The E and B intensities show directly the amount of emission in E and B, and they can be used for the identification and characterization of local features, which is obscured in the normal E and B mode maps. Note that if the EB angular power spectrum is negligible compared to the EE and BB angular power spectrum, then statistically, we get $\langle P_E^2 + P_B^2 \rangle = \langle P^2 \rangle$.

First we check the Planck 353 GHz dust polarization map, which has a relatively high resolution. We use the original resolution and choose the well known Large Magellanic Cloud (LMC) region as an example to plot three polarization maps of the original polarization and the E, B families respectively in figure 1. We can see an onion-like polarization pattern in the E-family, and at least three point source like structures in the B-family; however, both are hard to see in the original polarization map. We also show the normal scalar E and B mode maps in the same region, which does not show any special structure, and most importantly, we cannot get the polarization direction from a scalar E or B mode map. Thus, it is apparent that the E and B families can help to detect special structures in a polarization map.

We then examine the Planck 30 GHz polarization map, which has a original resolution of $N_{\text{side}} = 1024$, and we smooth it to 1° -FWHM to suppress the noises. Again three maps of the original polarization and the E and B families are shown in figure 2 for the position $(b, l) = (-31.2^\circ, 280^\circ)$ of the LMC region, respectively. We can see an interesting jet-like structure in the B-family, starting from the blue (cold) spot on the upper right corner of the black circle, and ejects towards the north-east direction. This structure is also marginally visible in the original polarization map, but is completely missing in the E-family. Therefore, special structures can be much more visible in the E or B family than in the original polarization map.

Next in figure 3, we focus on the $(b, l) = (-30.0^\circ, 279.2^\circ)$ and $(b, l) = (-32.1^\circ, 277.3^\circ)$ positions, which are both in the LMC region and close to the region of figure 2. In this two regions we see two nearly perfect spiral structure belonging to the B-family, which does not appear in 30, 44 or 100 GHz, and the amplitudes seem to be above the noise contribution. Therefore, they are unlikely to be the noise, CMB or synchrotron emission. One possibility is that they are due to the Anomalous microwave emission (AME). If this is true, then there should be some hidden mechanism that is able to create nearly pure B-mode polarization in AME.

Next in figure 4, we focus on the $(b, l) = (-32.0^\circ, 276.2^\circ)$ position in the LMC region, on the right of the lower part in figure 3. In this region we see another ejecting structure that is very similar to figure 2; however, the input map is Planck 353 GHz rather than 30 GHz; thus it is almost certainly due to the thermal dust emission. According to the similarity of the structures, a reasonable guess is that the structure in figure 2 is probably also associated to the dust emission. However, dust polarization in 30 GHz can only be AME (spinning or magnetic dust emissions). This again requires a mechanism that can create B-family polarization in the AME.

Then we focus on the ejecting structure in figure 2 and compare it for eight different bands from WMAP and Planck, including the WMAP K-band (22.8 GHz) and the Planck 30, 44 70, 100, 143, 217 and 353 GHz bands. The K to 70 GHz bands are re-beamed to 1° FWHM, and the higher bands are re-beamed to $30'$. The results are shown in figure 5. From this figure, we can see that the structure is visible in all frequency bands from 22 to 353 GHz, no matter WMAP or Planck, which safely excludes the possibility of CMB, noise or systematics. The amplitude variation from K-band to 30 GHz is consistent with the synchrotron emission spectrum ($\beta \sim -3$), and the amplitude variation from 217 to 353 GHz is also consistent with a thermal dust spectrum of $\beta \sim 1.6$ and $T_{\text{dust}} \sim 16$ K. These facts tell us that this structure includes significant synchrotron and thermal dust polarization at the same time. Thus, we have the following conclusions: 1) The B-family nature is most likely coming from a B-type magnetic

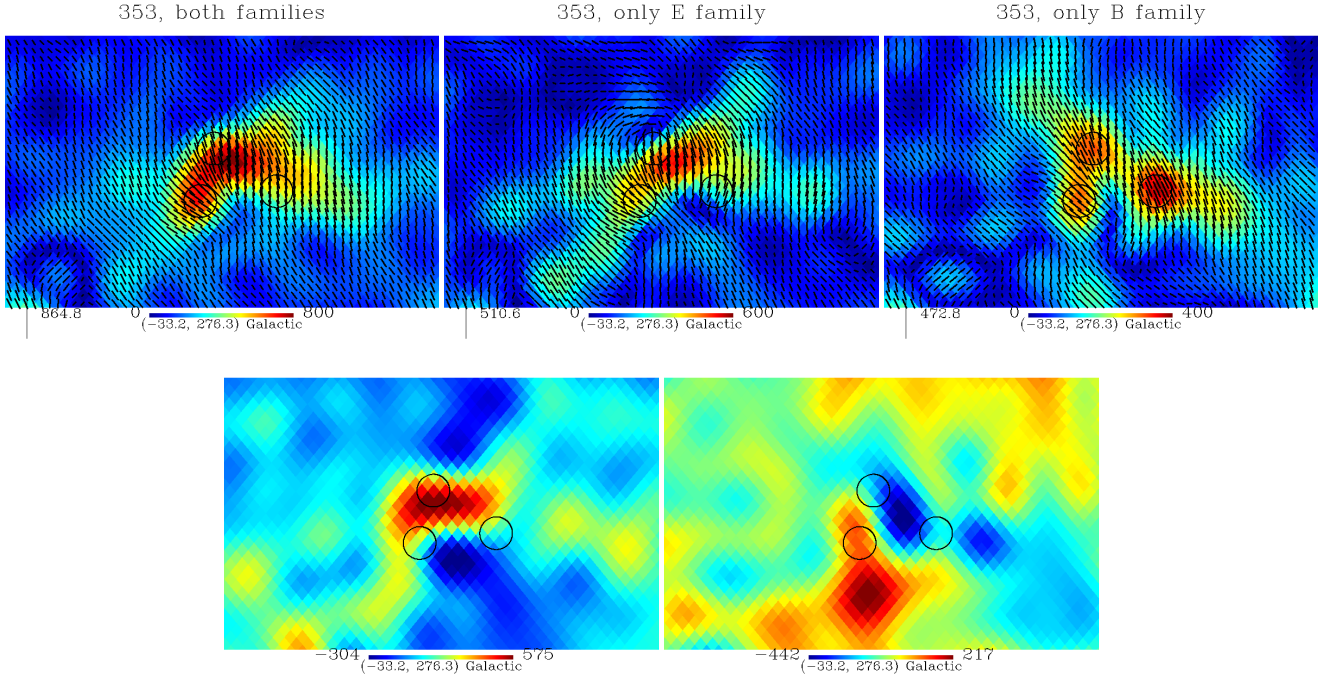


FIG. 1. The Planck 353 GHz polarization map around the LMC region at $N_{\text{side}} = 2048$. *Upper*, from left to right: the original polarization (including both the E and B families) and the E, B families. *Lower*, from left to right: the normal scalar E, B mode maps. At least three point source like structures can be seen in the B-family, and an onion-like polarization pattern can be seen in the E-family. However, both of them are hard to see in the original polarization map or any of the normal E or B maps. The diameter of black circle is 6 arcmin.

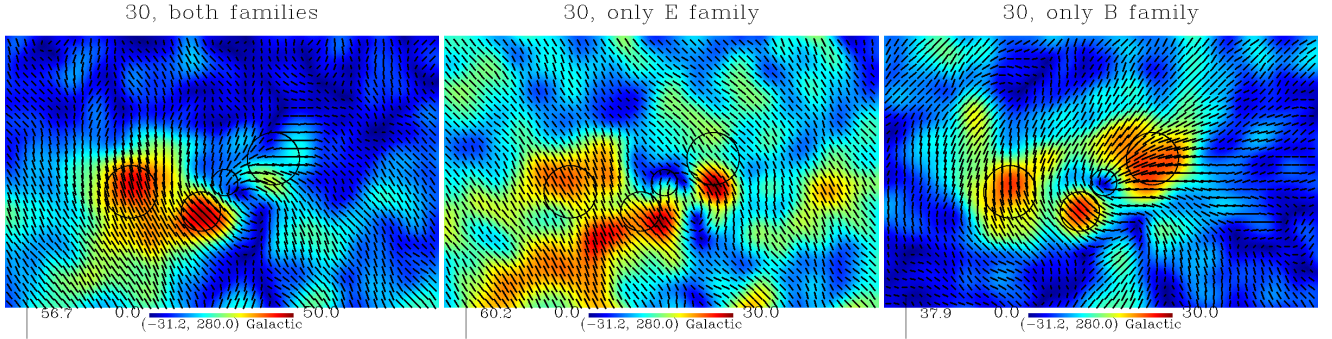


FIG. 2. The Planck 30 GHz polarization map at $N_{\text{side}} = 1024$, re-beamed from $32.23'$ to $40'$ to suppress the noise, and around $(b, l) = (-31.4^\circ, 280^\circ)$ in the LMC region. From left to right: the original polarization and the E, B family. An interesting jet-like structure can be seen clearly in the B-family, which starts from a small cold spot, and ejects towards the north-east direction. This structure is also marginally visible in the original polarization map, but is completely missing in the E-family. The diameter of the biggest black circle is 0.8° .

field distribution rather than a specific emission mechanism. 2) There should be a physical mechanism that can create such a B-type magnetic field distribution, and 3) the possibility of spin or magnetic dust emission cannot be completely excluded.

Immediately after figure 5, we perform three tests of the results: 1) Whether or not the results are affected by strong point sources. 2) Can we see similar structures in the original 353 GHz map (no smoothing, no EB-separation). 3) What is the structure look like when we rotate all polarizations by 90° . These test results are shown in figure 6. This figures tells us that: 1) The results in figures 5–6 are unaffected by point sources. 2) Similar polarization pattern can be seen even on the original polarization map (no smoothing, no EB-separation). 3) When we rotate all polarizations by 90° , it is still a ejecting structure but the direction is inverted. 4) The hot regions in B-family is apparently aligned with the hot regions in the original polarization. In all, the tests not only validates the results in figure 5, but also prefers the explanation that there is a foreground emission mechanism that prefers the B-mode.

We also perform a test of the E-major ($P_E > P_B$) and B-major ($P_E < P_B$) pixels by checking the fraction of such pixels in the regions of figures 2 and 4; and on the original resolution 353 GHz map. The fraction of E-major pixel is 43% for the region

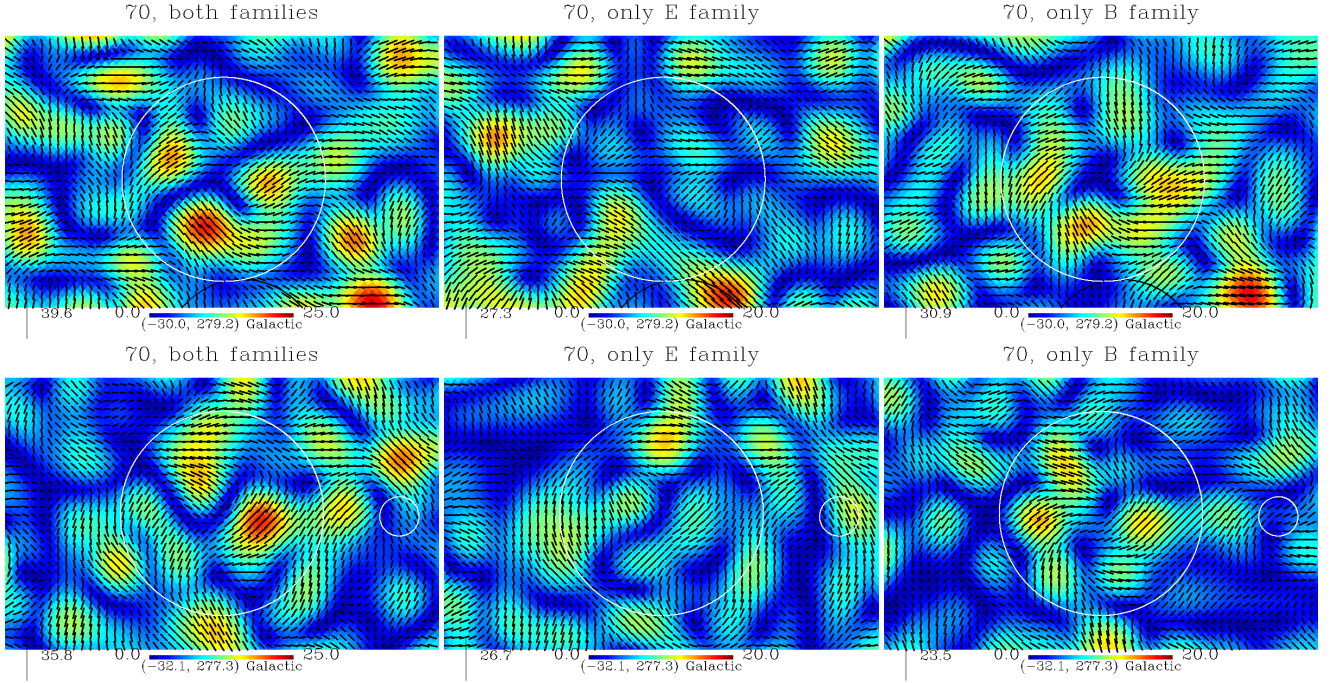


FIG. 3. The Planck 70 GHz polarization map at $N_{\text{side}} = 1024$ and re-beamed from $13.25'$ to $16'$ FWHM to suppress the noise. The two positions in the LMC region are presented. One is around $(b, l) = (-30.0^\circ, 279.2^\circ)$ (upper), and the other is around $(b, l) = (-32.1^\circ, 277.3^\circ)$ (lower). From left to right: the original polarization and the E, B family. Two nearly perfect spiral structures belonging to the B-mode can be seen in B-family and partially in the original polarization, but are of course missing in the E-family. Also note that both of them are cold (less polarized) in the center. The diameter of the white circle is 0.5° .

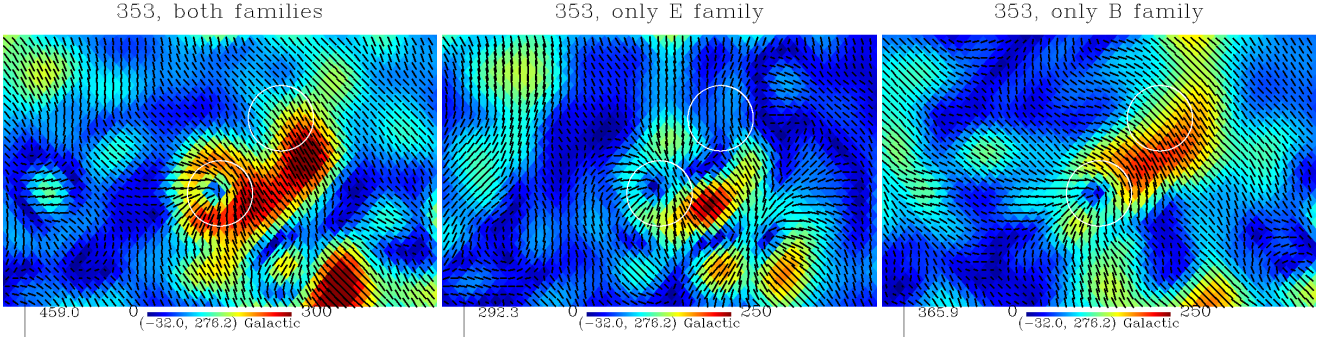


FIG. 4. Similar to figure 2 but for the Planck 353 GHz polarization map at $N_{\text{side}} = 2048$ without additional smoothing, showing position $(b, l) = (-32.07^\circ, 276.24^\circ)$ in the LMC region. A similar ejecting structure to figure 2 can be seen in the B-family at a much higher frequency.

in figure 2 and 33% for the region in figure 4, so both regions are dominated by the B-mode signals. The significance of such fractions are also tested by checking the same fraction in other regions of the same shape and size but centered at the $N_{\text{side}} = 8$ pixels and located above Gal-latitudes $|b| > 25^\circ$. Both tests show confidence levels of about $1 - a = 97\%$ that the B-mode dominance is significant, as illustrated by figure 7, which gives a joint confidence levels of about $1 - a = 99.9\%$.

We further check the regions in figures 4 and 6 using the foreground $H\alpha$ line emission and stellar continuum emission, as shown in figures 8 and 9. The results convincingly show that these regions are associated with bright and active foreground regions, and further prefers an explanation by foreground emission mechanism.

Finally, we show the fullsky Planck 30 GHz polarized map with the original and E, B family polarization in figure 10. There are many loop structures in the original polarization map, but with the E and B family decomposition, we can easily see that all loop-like structures are only from the E family, which was first discovered in [11] and whose mechanism was explained in [19]. We also point out that in figure 5 of a recent work [20], the mechanism of the Odd Radio Circle is found to be the same as the one found in in [19].

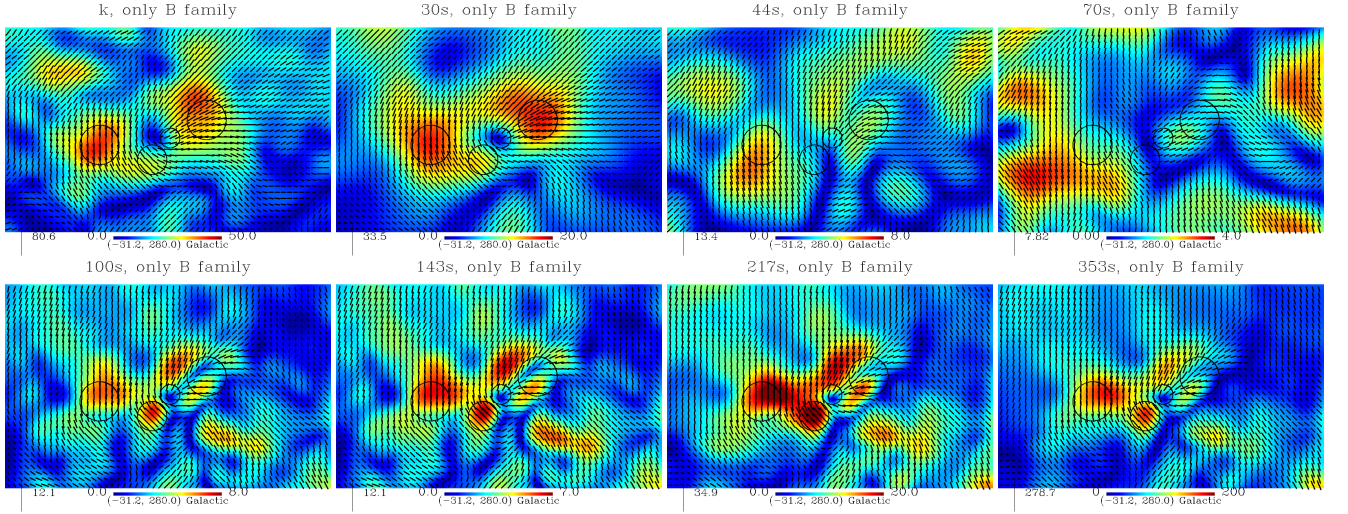


FIG. 5. Similar to figure 2 but focuses on the B-family ejecting structure in eight WMAP and Planck bands: *Upper*, from left-to-right: the WMAP K-band (22.8 GHz) and Planck 30, 44 70 bands; *Lower*, from left-to-right: the Planck 100, 143, 217 and 353 GHz bands.

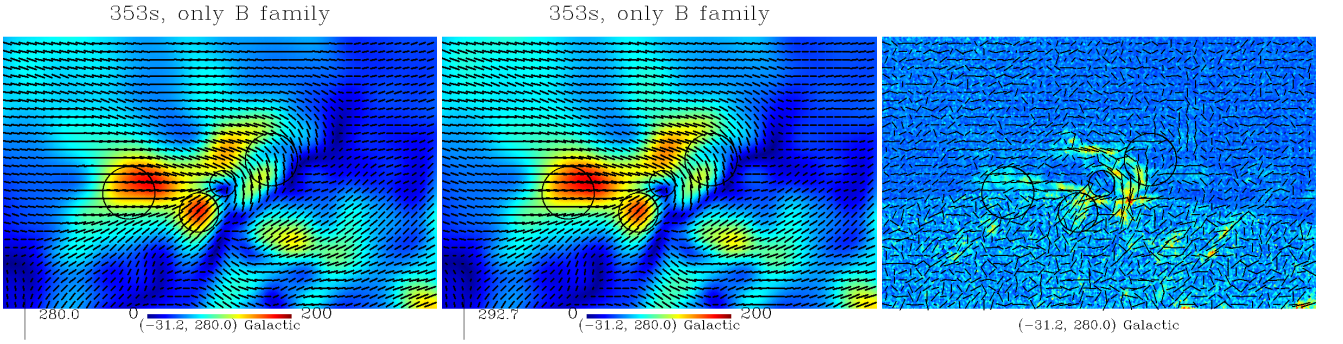


FIG. 6. Test of figure 5 for: 1) the point source effect, 2) self-consistency and 3) rotation of polarization by 90° . *Left*: Similar to the 353 GHz results in figure 5 but rotate all polarizations by 90° . *Middle*: Similar to the left panel but exclude 3% of the local region with strongest polarization intensities before any other operations, which shows no significant changes; thus the polarization patterns in figure 5 are nearly unaffected by point sources. *Right*: The original 353 GHz polarization map (also rotate the polarizations by 90°), no smoothing, no EB-separation. In this panel, we can see not only similar polarization pattern, but also alignment of the relatively hotter regions with the left panel. Which validates the B-family polarization patterns in figure 5 and strongly suggests there can be a foreground emission mechanism that prefers the B-mode.

B. Toy model of the mechanism of B-family emissions

In this section, we provide a toy model as an attempt to explain the B-family emissions shown in figures 2 and 4. The model is based on the model in [19] but gives an analytic solution at small angles. The model is briefly illustrated as follows:

Assume we stay at point $\mathbf{O} = (0, 0, 0)$, and a compact center object (star, supernova, blackhole, etc.) stays at $\mathbf{S} = (0, 0, 1)$. The line-of-sight is along the spherical polar direction (θ, φ) ; thus, a test point at distance d along the line-of-sight has Cartesian coordinates

$$\mathbf{P} = (d \sin \theta \cos \varphi, d \sin \theta \sin \varphi, d \cos \theta). \quad (42)$$

The vector from the compact object to the test point is

$$\begin{aligned} \mathbf{R} &= \mathbf{P} - \mathbf{S} = (d \sin \theta \cos \varphi, d \sin \theta \sin \varphi, d \cos \theta - 1) \\ |\mathbf{R}| &= r = \sqrt{1 - 2d \cos \theta + d^2}. \end{aligned} \quad (43)$$

Then we use cross products to define the natural reference frames for polarization [13] (normalized). The plus and minus axes

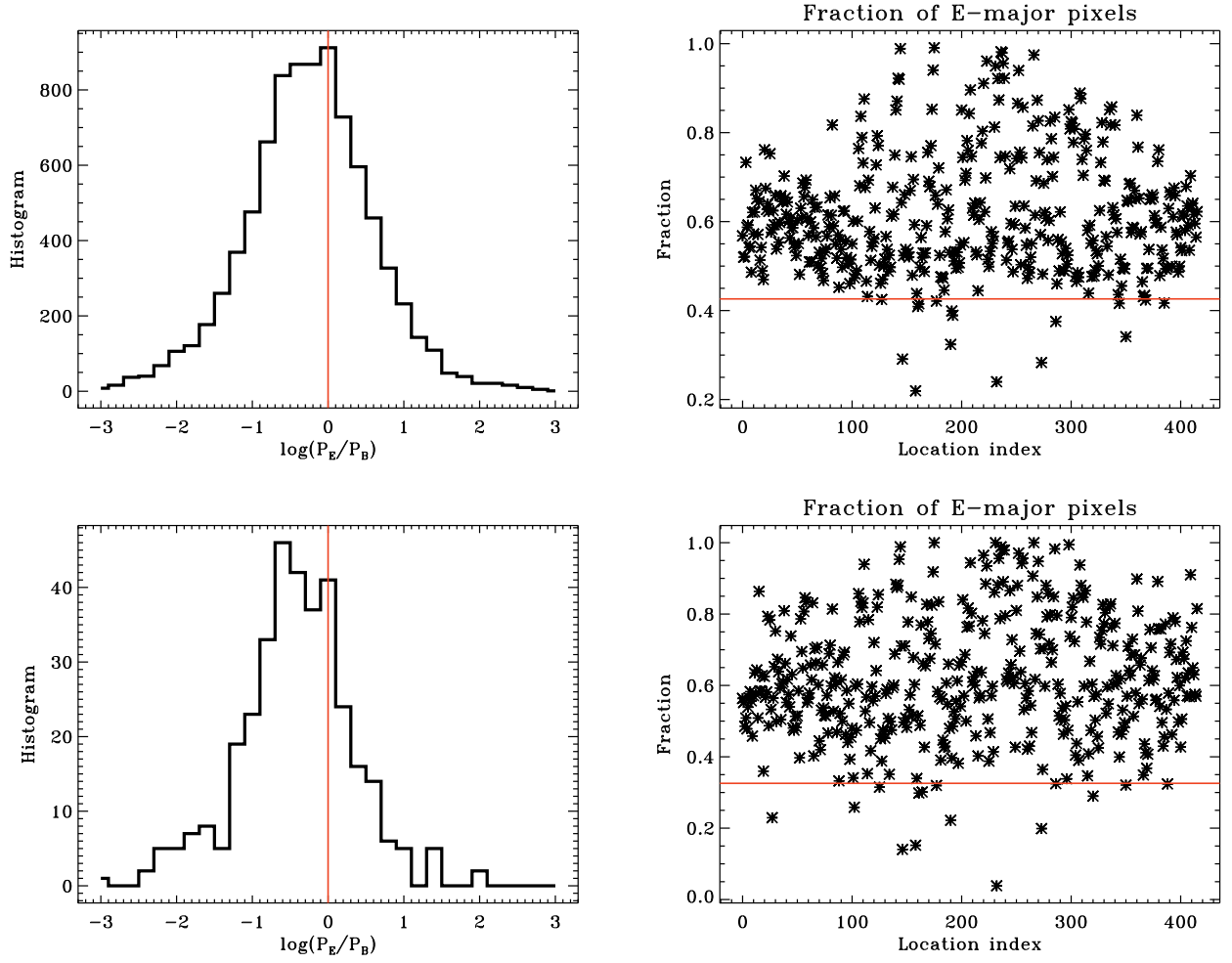


FIG. 7. Test of the E- or B-major pixels in the regions of figure 2 (upper) and figure 4 (lower). *Left*: The histogram of $\log(P_E/P_B)$ in the corresponding regions. *Right*: The fraction of E-major pixel in the region (the red line) compared with other regions of the same size and on the same map, located above Gal-latitudes $|b| > 25^\circ$ and centered at the $N_{side} = 8$ pixels.

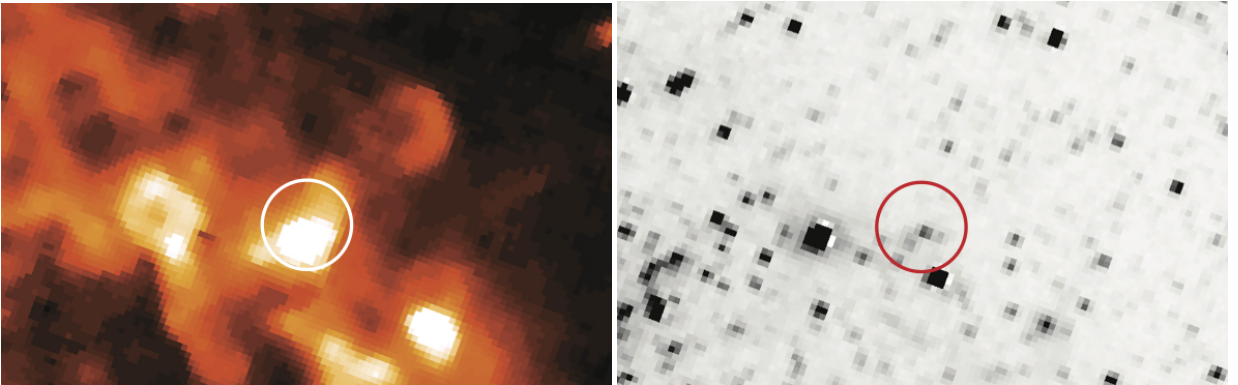


FIG. 8. The foreground $H\alpha$ line emission (*left*) and stellar continuum emission (*right*) images of the northern region of LMC in Galactic coordinate system with the galactic north pole to the top of the figures. Both images cover the same area as that in Figure 4. The circle with a 0.1° radius in each plot with marks the same corresponding location of the sky. The circle coincides with the emission region LH 120-N 64 [16]. The data presented here are obtained from The Southern H-Alpha Sky Survey Atlas [17].

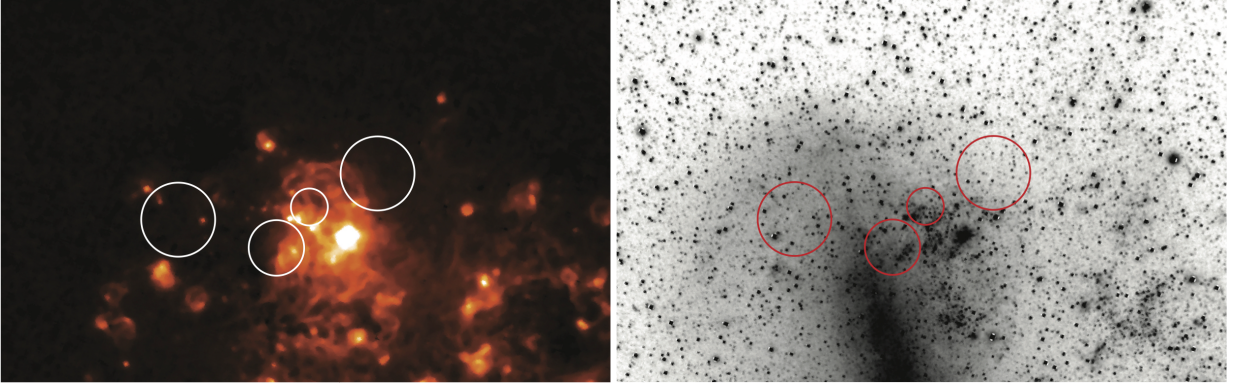


FIG. 9. The foreground $H\alpha$ line emission (*left*) and stellar continuum emission (*right*) images of the south-east region of LMC in Galactic coordinate system with the galactic north pole to the top of the figures. Both images cover the same area as that in Figure 6 and the circles within mark the same corresponding locations of the sky. Several young star clusters [18] associated with nebulae NGC 2080, NGC 2085, and NGC 2086 reside in between the two circles in the central region of the plot. The bright source in the $H\alpha$ image is 30 Doradus, a giant H II region in LMC. The data presented here are obtained from The Southern H-Alpha Sky Survey Atlas [17].

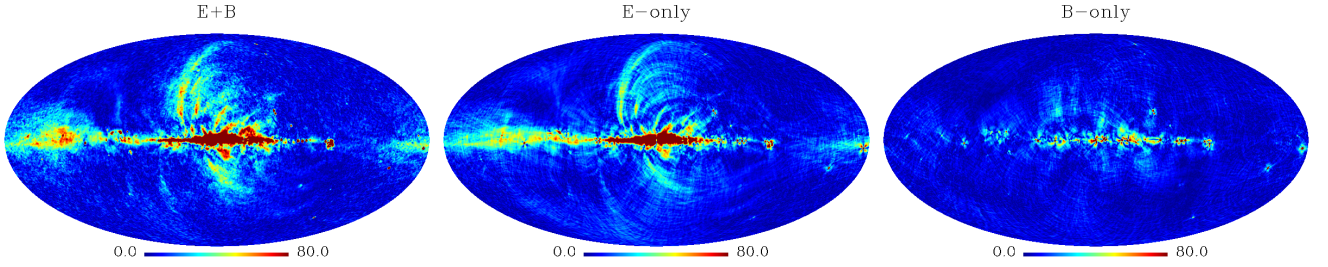


FIG. 10. The fullsky Planck 30 GHz polarization map at $N_{\text{side}} = 1024$ and smoothed to 1° , for: the original polarization (left, including both the E and B families), the E-family (middle) and the B-family (right). Apparently, all loop-like structures appear only in the E family, which was discovered in [11] and explained in [19].

for the Q-Stokes parameters are \mathbf{A}_\pm :

$$\begin{aligned} \mathbf{A}_+ &= \frac{\mathbf{P} \times \mathbf{S}}{d \sin \theta} = (\sin \varphi, -\cos \varphi, 0) \\ \mathbf{A}_- &= \frac{\mathbf{P} \times \mathbf{A}_+}{d} = (\cos \theta \cos \varphi, \cos \theta \sin \varphi, -\sin \theta). \end{aligned} \quad (44)$$

As the first step, we assume the background magnetic field is smooth at small scales, and its projection on \mathbf{R} (radial component) is erased by the shock wave or stellar wind. Then the initial and resulting magnetic fields are

$$\begin{aligned} \mathbf{B}_0 &= b_0(\sin \theta' \cos \varphi', \sin \theta' \sin \varphi', \cos \theta') \\ \mathbf{B} &= \mathbf{B}_0 - (\mathbf{B}_0 \cdot \mathbf{R}) \frac{\mathbf{R}}{r}, \end{aligned} \quad (45)$$

where \mathbf{B}_0 is the initial magnetic field, (θ', φ') is the direction of \mathbf{B}_0 in the spherical polar coordinate system, and \mathbf{B} is the resulting magnetic field. Then we compute the projection of the magnetic field on the \mathbf{A}_\pm axes as B_\pm :

$$\begin{aligned} B_+ &= \mathbf{B} \cdot \mathbf{A}_+ = \sin \theta' \sin(\varphi - \varphi') \\ B_- &= \mathbf{B} \cdot \mathbf{A}_- = \frac{-(d - \cos \theta)(d \cos \theta' \sin \theta + (1 - d \cos \theta) \cos(\varphi - \varphi') \sin \theta')}{1 - 2d \cos \theta + d^2}. \end{aligned} \quad (46)$$

If the polarization is perpendicular to the magnetic field, then the Q-stokes parameter is proportional to the power (square) difference: $Q \propto B_-^2 - B_+^2$, whereas for parallel polarizations the Q-stokes parameter is proportional to $Q \propto B_+^2 - B_-^2$.

Because in the natural reference system, the Q-Stokes parameter corresponds to the E-mode, the fraction of the E-mode in the

total polarization can be described by

$$f_E = \pm \frac{B_+^2 - B_-^2}{B_+^2 + B_-^2} \in [-1, 1]. \quad (47)$$

If f_E is close to ± 1 , then the polarization is dominated by the E-family. If f_E is close to zero, then the polarization is dominated by the B-family.

Now we introduce the small angle approximation: $\theta \ll 1$, which means the line-of-sight is not far from the center compact object. Then eq. (45) is simplified to:

$$\begin{aligned} B_+ &= \mathbf{B} \cdot \mathbf{A}_+ = \sin \theta' \sin(\varphi - \varphi') \\ B_- &= \mathbf{B} \cdot \mathbf{A}_- \approx \sin \theta' \cos(\varphi - \varphi'). \end{aligned} \quad (48)$$

Thus we have

$$f_E \approx \pm \frac{B_+^2 - B_-^2}{B_+^2 + B_-^2} = \pm \cos 2(\varphi - \varphi') \quad (49)$$

Therefore, if the following conditions are satisfied:

1. The background magnetic field does not change significantly at small scales.
2. For some reason, the effect of shock wave or stellar wind is asymmetric. This includes at least two possibilities: a) The shockwave or stellar wind itself is asymmetric. b) The shock wave or stellar wind is symmetric, but the interstellar medium is asymmetric.
3. The major direction of effect is roughly 45° apart from the direction of the smooth background magnetic field (both consider only the projection to the xy -plane), i.e., $\cos 2(\varphi - \varphi') \approx 0$.

Then the polarization will be dominated by the B-family.

By checking the foreground H α line emission and stellar continuum emission in figures 8 and 9 and comparing them with the polarization structures in figures 2 and 4, we can see asymmetric bubble-like structures in the former, which is qualitatively consistent with the B-family structure in the latter, especially the direction of the bubble-like structures' shell. This fact indicates that the above toy model is at least qualitatively reasonable.

VI. DISCUSSION

Earlier works [11, 12, 19, 21] have established the E/B decomposition as a non-local operation, which can be mathematically expressed in terms of an integral convolution in pixel space, and the corresponding convolution kernels have been calculated and visualized. In this work, we return to the E–B decomposition theory, and, working in the space of the Stokes parameters Q and U , show how the operation can be formulated using quaternion multiplication. The quaternion algebra naturally accommodates the harmonic-space E/B modes, and the relations between all relevant quantities can be written compactly as products of quaternion matrices. For this purpose, we depend on the different types of quaternion conjugation, which are described in the appendix. Apart from its mathematical concision and beauty, the quaternion representation of the E/B decomposition can be developed into a general quaternionic eigenproblem, where the different spins are related to the eigenvectors and the parities to the eigenvalues.

As example of applications, we also study the Stoke-space E/B modes and associated estimators in the polarized foregrounds analysis, which discovers several interesting foreground structures in the E- and B-families; and give reasonable explanations of their mechanisms (see also [19]), which was also used recently to explain the mechanism of the Odd Radio Circle [20].

ACKNOWLEDGMENTS

This work is supported in part by the National Key R&D Program of China (2021YFC2203100, 2021YFC2203104) and the Anhui project Z010118169.

Appendix A: The system of quaternion multiplication

A quaternion is formed by four real numbers or, equivalently, by two complex numbers as follows:

$$\mathbf{q} = (a, b, c, d) = a + b\mathbf{i} + c\mathbf{j} + d\mathbf{k} = z_1 + z_2\mathbf{j}, \quad (\text{A1})$$

where $z_1 = a + b\mathbf{i}$ and $z_2 = c + d\mathbf{i}$, and $\mathbf{i}, \mathbf{j}, \mathbf{k}$ are three imaginary units that satisfy:

1. $\mathbf{i}\mathbf{i} = \mathbf{j}\mathbf{j} = \mathbf{k}\mathbf{k} = -1$.
2. $\mathbf{i}\mathbf{j} = \mathbf{k}, \mathbf{j}\mathbf{k} = \mathbf{i}$ and $\mathbf{k}\mathbf{i} = \mathbf{j}$.
3. $\mathbf{i}\mathbf{j} = -\mathbf{j}\mathbf{i}, \mathbf{j}\mathbf{k} = -\mathbf{k}\mathbf{j}$ and $\mathbf{k}\mathbf{i} = -\mathbf{i}\mathbf{k}$.

The elements attached to \mathbf{i}, \mathbf{j} , and \mathbf{k} are called the imaginary parts of a quaternion (or vector part), and the rest is called the real or scalar part of a quaternion. With these rules, it is easy to see that the multiplication of two quaternions $q_1 = (a_1, b_1, c_1, d_1)$ and $q_2 = (a_2, b_2, c_2, d_2)$ is

$$\begin{aligned} q_1 q_2 = & (a_1 a_2 - b_1 b_2 - c_1 c_2 - d_1 d_2) + \\ & (a_1 b_2 + b_1 a_2 + c_1 d_2 - d_1 c_2) \mathbf{i} + \\ & (a_1 c_2 - b_1 d_2 + c_1 a_2 + d_1 b_2) \mathbf{j} + \\ & (a_1 d_2 + b_1 c_2 - c_1 b_2 + d_1 a_2) \mathbf{k}, \end{aligned} \quad (\text{A2})$$

where the elements of the first quaternion are aligned vertically, and the elements of the second quaternion are placed in a way shown in figure 11:

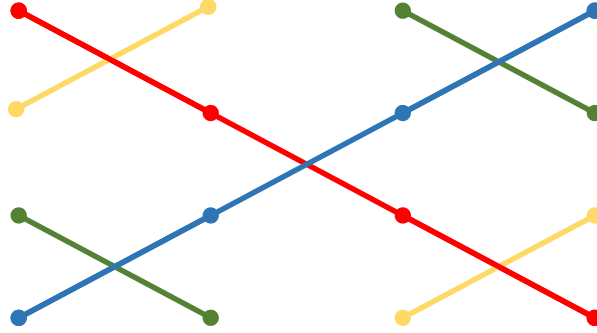


FIG. 11. Placement of the second quaternion's elements in a quaternion multiplication.

1. The system of quaternion conjugates

Unlike the complex numbers that have only one conjugate, the quaternions have seven different conjugates. Because this is seldom mentioned in literature, in this work we define a symbol for these seven conjugates as \mathbf{q}^{*x} , where x is a three-bit binary number with the bits corresponding to \mathbf{i}, \mathbf{j} , and \mathbf{k} respectively. If the value of one bit is equal to 1, then the corresponding imaginary part will be inverted. For example, $(a, b, c, d)^{*100} = (a, -b, c, d)$. It is worth to mention that \mathbf{q}^{*111} can also be shortened as \mathbf{q}^* , which is the most widely used quaternion conjugate that inverts all imaginary parts simultaneously.

Below we provide examples of how the seven quaternion conjugates are connected to actual transforms, but note that they are apparently not the only possibilities:

1. Type-001 (Type-1, symbol: \mathbf{q}^{*001} or \mathbf{q}^{*1}) conjugate: $z_1 + z_2\mathbf{j} \longrightarrow z_1 + z_2^*\mathbf{j}$.
2. Type-010 (Type-2, symbol: \mathbf{q}^{*010} or \mathbf{q}^{*2}) conjugate: $z_1 + z_2\mathbf{j} \longrightarrow z_1 - z_2^*\mathbf{j}$.
3. Type-011 (Type-3, symbol: \mathbf{q}^{*011} or \mathbf{q}^{*3}) conjugate: $z_1 + z_2\mathbf{j} \longrightarrow z_1 - z_2\mathbf{j}$.
4. Type-100 (Type-4, symbol: \mathbf{q}^{*100} or \mathbf{q}^{*4}) conjugate: $z_1 + z_2\mathbf{j} \longrightarrow z_1^* + z_2\mathbf{j}$.

5. Type-101 (Type-5, symbol: q^{*101} or q^{*5}) conjugate: $z_1 + z_2j \longrightarrow z_1^* + z_2^*j$.
6. Type-110 (Type-6, symbol: q^{*110} or q^{*6}) conjugate: $z_1 + z_2j \longrightarrow z_1^* - z_2^*j$.
7. Type-111 (Type-7, symbol: q^{*111} or q^{*7}) conjugate: $z_1 + z_2j \longrightarrow z_1^* - z_2j$.

For convenience and as shown above, the quaternion conjugates can possibly be shortened as $*_{x'}$, where x' is the decimal value of the binary number x . However, the binary symbol is recommended because it makes the following rule more clear: Let $x_{1,2,3}$ be the values of the three digits of x , so they are either 1 or 0; then by eq. (A2) it is easy to prove that

$$\begin{aligned} \text{If } x_1 + x_2 + x_3 = \text{Odd} \text{ then : } (q_1q_2)^{*x} &= q_2^{*x}q_1^{*x}, \\ \text{If } x_1 + x_2 + x_3 = \text{Even} \text{ then : } (q_1q_2)^{*x} &= q_1^{*x}q_2^{*x}. \end{aligned} \quad (\text{A3})$$

When $x_1 + x_2 + x_3$ is odd/even, the corresponding conjugate is called an odd/even conjugate. The above equation means, for the quaternions, odd and even conjugates follow different combinations of the distributive and commutative laws. It is also easy to see that the combination of odd conjugates can give both odd and even conjugates, but the combination of even conjugates will *not* give an odd conjugate.

From eq. (A3), it is also easy to prove that, for an odd conjugate, the corresponding imaginary part will be erased in the quaternion multiplication qq^{*x} , for example, when $q = (a, b, c, d)$, we have:

$$\begin{aligned} qq^{*100} &= (a^2 + b^2 - c^2 - d^2, \mathbf{0}, 2ac - 2bd, 2ad + 2bc) \\ qq^{*111} &= (a^2 + b^2 + c^2 + d^2, \mathbf{0}, \mathbf{0}, \mathbf{0}). \end{aligned} \quad (\text{A4})$$

However, for an even conjugate, the corresponding imaginary parts are erased not in a direct multiplication, but in the combination $qq^{*x} + q^{*x}q$, like:

$$\begin{aligned} qq^{*110} &= (a^2 + b^2 + c^2 - d^2, 2cd, -2bd, 2ad) \\ qq^{*110} + q^{*110}q &= 2(a^2 + b^2 + c^2 - d^2, \mathbf{0}, \mathbf{0}, 2ad) \end{aligned} \quad (\text{A5})$$

Therefore, the quaternions have at least three independent parity states – one for each imaginary part. Each single conjugate ($x_1 + x_2 + x_3 = 1$) will help to erase one parity state in the multiplication because we have $0 = \pm 0$ at the same time.

2. The system of quaternion matrix multiplication

The algebra of quaternion matrix has been discussed in detail by [22]. However, the order problem in quaternion matrix multiplication has not been studied, which will be discussed below.

Let $\mathbf{a} = (a_1, a_2, a_3, a_4)$, $\mathbf{b} = (b_1, b_2, b_3, b_4)$ and $\mathbf{x} = (x_1, x_2, x_3, x_4)$ be quaternions, and $\mathbf{A} \equiv \mathbf{a}_{ij}$, $\mathbf{B} \equiv \mathbf{b}_{jk}$, $\mathbf{X} \equiv \mathbf{x}_k$ be two $n \times n$ square matrices and one $n \times 1$ column matrix of quaternions. Then a naive definition of the matrix multiplication \mathbf{ABX} is

$$\mathbf{ABX} \xrightarrow{\text{naive}} \sum_{jk} \mathbf{a}_{ij} \mathbf{b}_{jk} \mathbf{x}_k. \quad (\text{A6})$$

However, because quaternion multiplication is non-commutative, there are actually six quaternion orders for the about matrix multiplication:

$$\begin{aligned} (\mathbf{ABX})_{012} &\equiv \sum_{jk} \mathbf{a}_{ij} \mathbf{b}_{jk} \mathbf{x}_k, & (\mathbf{ABX})_{021} &\equiv \sum_{jk} \mathbf{a}_{ij} \mathbf{x}_k \mathbf{b}_{jk}, \\ (\mathbf{ABX})_{102} &\equiv \sum_{jk} \mathbf{b}_{jk} \mathbf{a}_{ij} \mathbf{x}_k, & (\mathbf{ABX})_{120} &\equiv \sum_{jk} \mathbf{b}_{jk} \mathbf{x}_k \mathbf{a}_{ij}, \\ (\mathbf{ABX})_{201} &\equiv \sum_{jk} \mathbf{x}_k \mathbf{a}_{ij} \mathbf{b}_{jk}, & (\mathbf{ABX})_{210} &\equiv \sum_{jk} \mathbf{x}_k \mathbf{b}_{jk} \mathbf{a}_{ij}. \end{aligned} \quad (\text{A7})$$

Some of the orders can be implemented by changing the order of matrix multiplication with a proper transposing; however, this is not always possible, like order-120, because the rule of matrix multiplication does not allow a column matrix \mathbf{X} to be placed between two square matrices \mathbf{A} and \mathbf{B} . Therefore, in order to properly define the quaternion matrix multiplication, we have to find out a way to separate the order of quaternion multiplication from the order of matrix multiplication.

According to eq. (A2), it is easy to write the quaternion multiplication of \mathbf{a} and \mathbf{x} in a matrix forms:

$$\begin{aligned}\mathbf{a}\mathbf{x} &\equiv \begin{pmatrix} a_1 & -a_2 & -a_3 & -a_4 \\ a_2 & a_1 & -a_4 & a_3 \\ a_3 & a_4 & a_1 & -a_2 \\ a_4 & -a_3 & a_2 & a_1 \end{pmatrix} \cdot \begin{pmatrix} x_1 \\ x_2 \\ x_3 \\ x_4 \end{pmatrix} = \mathbf{a}_L \cdot \mathbf{x}_o \\ \mathbf{x}\mathbf{a} &\equiv \begin{pmatrix} a_1 & -a_2 & -a_3 & -a_4 \\ a_2 & a_1 & a_4 & -a_3 \\ a_3 & -a_4 & a_1 & a_2 \\ a_4 & a_3 & -a_2 & a_1 \end{pmatrix} \cdot \begin{pmatrix} x_1 \\ x_2 \\ x_3 \\ x_4 \end{pmatrix} = \mathbf{a}_R \cdot \mathbf{x}_o,\end{aligned}\tag{A8}$$

where subscripts “ L/R ” means to augment each quaternion to its left/right 4×4 real matrix, and subscript “ o ” means to augment each quaternion to its 4×1 real column matrix form, and the augmentations work for both quaternion and quaternion matrix. The above equations show how to write quaternion multiplication with different orders with a fixed-order matrix multiplication, which is exactly what we need. Now the six quaternion orders of \mathbf{ABX} can be written as

$$\begin{aligned}(\mathbf{ABX})_{012} &\equiv \sum_{jk} \mathbf{a}_{ij} \mathbf{b}_{jk} \mathbf{x}_k \equiv \mathbf{A}_L \mathbf{B}_L \mathbf{X}_o, & (\mathbf{ABX})_{021} &\equiv \sum_{jk} \mathbf{a}_{ij} \mathbf{x}_k \mathbf{b}_{jk} \equiv \mathbf{A}_L \mathbf{B}_R \mathbf{X}_o, \\ (\mathbf{ABX})_{102} &\equiv \sum_{jk} \mathbf{b}_{jk} \mathbf{a}_{ij} \mathbf{x}_k \equiv (\mathbf{A}_R \mathbf{B}_o)_L \mathbf{X}_o, & (\mathbf{ABX})_{120} &\equiv \sum_{jk} \mathbf{b}_{jk} \mathbf{x}_k \mathbf{a}_{ij} \equiv \mathbf{A}_R \mathbf{B}_L \mathbf{X}_o, \\ (\mathbf{ABX})_{201} &\equiv \sum_{jk} \mathbf{x}_k \mathbf{a}_{ij} \mathbf{b}_{jk} \equiv (\mathbf{A}_L \mathbf{B}_o)_R \mathbf{X}_o, & (\mathbf{ABX})_{210} &\equiv \sum_{jk} \mathbf{x}_k \mathbf{b}_{jk} \mathbf{a}_{ij} \equiv (\mathbf{A}_R \mathbf{B}_o)_R \mathbf{X}_o.\end{aligned}\tag{A9}$$

By this way, the orders of quaternion multiplication and matrix multiplication are separated, and we are free to use any appropriate orders to solve a problem.

Appendix B: Quick reference of the E and B family decomposition with quaternions

Here we summarize the main results of the E and B family decomposition for a quick reference:

Given the basic spin-2 spherical harmonic decomposition:

$$a_{\pm 2, \ell m} = \int (Q \pm U \mathbf{i}) [{}_2 Y_{\ell m}^*] d\mathbf{n},\tag{B1}$$

The E and B mode spherical harmonic coefficients are defined as

$$\begin{aligned}a_{E, \ell m} &= \frac{a_{2, \ell m} + a_{-2, \ell m}}{2} \\ a_{B, \ell m} \mathbf{i} &= \frac{a_{2, \ell m} - a_{-2, \ell m}}{2}.\end{aligned}\tag{B2}$$

By defining

$$F_{+, \ell m} = \frac{1}{2} ({}_2 Y_{\ell m} + {}_{-2} Y_{\ell m}) \quad F_{-, \ell m} = \frac{1}{2} ({}_2 Y_{\ell m} - {}_{-2} Y_{\ell m}),\tag{B3}$$

we get the E and B families as

$$\begin{cases} Q_E = \sum_{\ell m} a_{E, \ell m} F_{+, \ell m} \\ U_E \mathbf{i} = \sum_{\ell m} a_{E, \ell m} F_{-, \ell m} \\ Q_B = \sum_{\ell m} (a_{B, \ell m} \mathbf{i}) F_{-, \ell m} \\ U_B \mathbf{i} = \sum_{\ell m} (a_{B, \ell m} \mathbf{i}) F_{+, \ell m} \end{cases}.\tag{B4}$$

The harmonic domain summation of F_{\pm} is

$$\begin{aligned}\sum_{\ell m} F_{+, \ell m}(\mathbf{n}) F_{+, \ell m}^*(\mathbf{n}') &= \text{Re}(\mathcal{Y}_+); & \sum_{\ell m} F_{+, \ell m}(\mathbf{n}) F_{-, \ell m}^*(\mathbf{n}') &= \mathbf{i} \text{Im}(\mathcal{Y}_-) \\ \sum_{\ell m} F_{-, \ell m}(\mathbf{n}) F_{-, \ell m}^*(\mathbf{n}') &= \text{Re}(\mathcal{Y}_-); & \sum_{\ell m} F_{-, \ell m}(\mathbf{n}) F_{+, \ell m}^*(\mathbf{n}') &= \mathbf{i} \text{Im}(\mathcal{Y}_+),\end{aligned}\tag{B5}$$

where \mathcal{F}_\pm are defined as

$$\begin{aligned}\mathcal{F}_+(\mathbf{n}, \mathbf{n}') &= \sum_\ell \sqrt{\frac{2\ell+1}{4\pi}} \frac{{}_2Y_{\ell,-2}(\beta, \alpha) + {}_2Y_{\ell,2}(\beta, \alpha)}{2} \\ \mathcal{F}_-(\mathbf{n}, \mathbf{n}') &= \sum_\ell \sqrt{\frac{2\ell+1}{4\pi}} \frac{{}_2Y_{\ell,-2}(\beta, \alpha) - {}_2Y_{\ell,2}(\beta, \alpha)}{2}.\end{aligned}\tag{B6}$$

Then we define five quaternions straightforwardly:

$$\begin{aligned}\mathcal{F}_{\ell m} &= F_{+,\ell m} + F_{-,\ell m} \mathbf{j} \\ \mathcal{G} &= \mathcal{F}_+ + \mathcal{F}_- \mathbf{j} \\ \mathcal{D} &= P_E + P_B \mathbf{j} \\ \mathcal{A}_{\ell m} &= a_{E,\ell m} + (a_{B,\ell m} \mathbf{i}) \mathbf{j} = a_{E,\ell m} + a_{B,\ell m} \mathbf{k} \\ \mathcal{P} &= Q + (U \mathbf{i}) \mathbf{j} = Q + U \mathbf{k},\end{aligned}\tag{B7}$$

where $\mathcal{F}_{\ell m}$ is the base function of EB-decomposition, \mathcal{G} is the pixel domain convolution kernel, \mathcal{D} is the expected pixel domain EB-family, $\mathcal{A}_{\ell m}$ is the harmonic domain EB-coefficient, and \mathcal{P} is a two-element quaternion containing the pixel domain Q and U Stokes parameters. The matrix forms of these quaternions are expressed in bold letters. With the above definition, we have:

1. The forward and backward transforms between \mathcal{P} (containing the input Q, U) and \mathcal{A} (containing the resulting $a_{E,\ell m}, a_{B,\ell m}$) is given by the following quaternion matrix equations:

$$\begin{aligned}\mathcal{A} &= \mathcal{F}^{H_{101}} \mathcal{P} \\ \mathcal{P} &= \mathcal{F}^{*_{010}} \mathcal{A},\end{aligned}\tag{B8}$$

where $^{H_{101}}$ and $^{*_{010}}$ are quaternion conjugates defined in Appendix A 1.

2. The pixel-pixel domain decomposition of the E and B families is

$$\mathcal{D} = \mathcal{G} \mathcal{P},\tag{B9}$$

3. The forward and backward transforms between the pixel domain E and B families and $a_{E,\ell m}, a_{B,\ell m}$ are given in the following quaternion matrix form, where $\mathcal{Y}_2 = {}_2Y_{\ell m}(\mathbf{n})$ is the matrix form of ${}_2Y_{\ell m}(\mathbf{n})$:

$$\begin{aligned}\mathcal{D} &= \mathcal{Y}_2 \mathcal{A} \\ \mathcal{A} &= \mathcal{Y}_2^H \mathcal{D},\end{aligned}\tag{B10}$$

-
- [1] G. Hinshaw, D. Larson, E. Komatsu, D. N. Spergel, C. L. Bennett, J. Dunkley, M. R. Nolta, M. Halpern, R. S. Hill, N. Odegard, L. Page, K. M. Smith, J. L. Weiland, B. Gold, N. Jarosik, A. Kogut, M. Limon, S. S. Meyer, G. S. Tucker, E. Wollack, and E. L. Wright, Nine-year Wilkinson Microwave Anisotropy Probe (WMAP) Observations: Cosmological Parameter Results, *Astrophys. J.Suppl.* **208**, 19 (2013), arXiv:1212.5226 [astro-ph.CO].
 - [2] Planck Collaboration, N. Aghanim, Y. Akrami, M. Ashdown, J. Aumont, C. Baccigalupi, M. Ballardini, A. J. Banday, R. B. Barreiro, and N. Bartolo, Planck 2018 results. VI. Cosmological parameters, arXiv e-prints, arXiv:1807.06209 (2018), arXiv:1807.06209 [astro-ph.CO].
 - [3] BICEP2/Keck Collaboration, Planck Collaboration, P. A. R. Ade, N. Aghanim, Z. Ahmed, R. W. Aikin, K. D. Alexander, M. Arnaud, J. Aumont, C. Baccigalupi, and et al., Joint Analysis of BICEP2/Keck Array and Planck Data, *Physical Review Letters* **114**, 101301 (2015), arXiv:1502.00612.
 - [4] BICEP2 Collaboration, Keck Array Collaboration, P. A. R. Ade, Z. Ahmed, R. W. Aikin, K. D. Alexander, D. Barkats, S. J. Benton, C. A. Bischoff, J. J. Bock, R. Bowens-Rubin, J. A. Brevik, I. Buder, E. Bullock, V. Buza, J. Connors, J. Cornelison, B. P. Crill, M. Crumrine, M. Dierickx, L. Duband, C. Dvorkin, J. P. Filippini, S. Fliescher, J. Grayson, G. Hall, M. Halpern, S. Harrison, S. R. Hildebrandt, G. C. Hilton, H. Hui, K. D. Irwin, J. Kang, K. S. Karkare, E. Karpel, J. P. Kaufman, B. G. Keating, S. Kefeli, S. A. Kernasovskiy, J. M. Kovac, C. L. Kuo, N. A. Larsen, K. Lau, E. M. Leitch, M. Lueker, K. G. Megerian, L. Moncelsi, T. Namikawa, C. B. Netterfield, H. T. Nguyen, R. O'Brien, R. W. Ogburn, S. Palladino, C. Pryke, B. Racine, S. Richter, A. Schillaci, R. Schwarz, C. D. Sheehy, A. Soliman, T. St. Germaine, Z. K. Staniszewski, B. Steinbach, R. V. Sudiwala, G. P. Teply, K. L. Thompson, J. E. Tolan, C. Tucker, A. D. Turner, C. Umiltà, A. G. Vieregg, A. Wand ui, A. C. Weber, D. V. Wiebe, J. Willmert, C. L. Wong, W. L. K. Wu, H. Yang, K. W. Yoon, and C. Zhang, Constraints on Primordial Gravitational Waves Using Planck, WMAP, and New BICEP2/Keck Observations through the 2015 Season, *Phys. Rev. Lett.* **121**, 221301 (2018), arXiv:1810.05216 [astro-ph.CO].

- [5] P. A. R. Ade, Z. Ahmed, M. Amiri, D. Barkats, R. B. Thakur, C. A. Bischoff, D. Beck, J. J. Bock, H. Boenish, E. Bullock, V. Buza, J. R. Cheshire, J. Connors, J. Cornelson, M. Crumrine, A. Cukierman, E. V. Denison, M. Dierickx, L. Duband, M. Eiben, S. Fatigoni, J. P. Filippini, S. Fliescher, N. Goeckner-Wald, D. C. Goldfinger, J. Grayson, P. Grimes, G. Hall, G. Halal, M. Halpern, E. Hand, S. Harrison, S. Henderson, S. R. Hildebrandt, G. C. Hilton, J. Hubmayr, H. Hui, K. D. Irwin, J. Kang, K. S. Karkare, E. Karpel, S. Kefeli, S. A. Kernasovskiy, J. M. Kovac, C. L. Kuo, K. Lau, E. M. Leitch, A. Lennox, K. G. Megerian, L. Minutolo, L. Monceli, Y. Nakato, T. Namikawa, H. T. Nguyen, R. O'Brient, R. W. Ogburn, S. Palladino, T. Prouve, C. Pryke, B. Racine, C. D. Reintsema, S. Richter, A. Schillaci, R. Schwarz, B. L. Schmitt, C. D. Sheehy, A. Soliman, T. S. Germaine, B. Steinbach, R. V. Sudiwala, G. P. Teply, K. L. Thompson, J. E. Tolan, C. Tucker, A. D. Turner, C. Umiltà, C. Vergès, A. G. Vieregge, A. Wandui, A. C. Weber, D. V. Wiebe, J. Willmert, C. L. Wong, W. L. K. Wu, H. Yang, K. W. Yoon, E. Young, C. Yu, L. Zeng, C. Zhang, and S. Zhang (BICEP/Keck Collaboration), Improved constraints on primordial gravitational waves using planck, wmap, and bicep/keck observations through the 2018 observing season, *Phys. Rev. Lett.* **127**, 151301 (2021).
- [6] M. Hazumi, J. Borrill, Y. Chinone, M. A. Dobbs, H. Fuke, A. Ghribi, M. Hasegawa, K. Hattori, M. Hattori, W. L. Holzapfel, Y. Inoue, K. Ishidoshiro, H. Ishino, K. Karatsu, N. Katayama, I. Kawano, A. Kibayashi, Y. Kibe, N. Kimura, K. Koga, E. Komatsu, A. T. Lee, H. Matsuhara, T. Matsumura, S. Mima, K. Mitsuda, H. Morii, S. Murayama, M. Nagai, R. Nagata, S. Nakamura, K. Natsume, H. Nishino, A. Noda, T. Noguchi, I. Ohta, C. Otani, P. L. Richards, S. Sakai, N. Sato, Y. Sato, Y. Sekimoto, A. Shimizu, K. Shinozaki, H. Sugita, A. Suzuki, T. Suzuki, O. Tajima, S. Takada, Y. Takagi, Y. Takei, T. Tomaru, Y. Uzawa, H. Watanabe, N. Yamasaki, M. Yoshida, T. Yoshida, and K. Yotsumoto, LiteBIRD: a small satellite for the study of B-mode polarization and inflation from cosmic background radiation detection, in *Space Telescopes and Instrumentation 2012: Optical, Infrared, and Millimeter Wave*, Proceedings of SPIE, Vol. 8442 (2012) p. 844219.
- [7] K. N. Abazajian, P. Adshead, Z. Ahmed, S. W. Allen, D. Alonso, K. S. Arnold, C. Baccigalupi, J. G. Bartlett, N. Battaglia, B. A. Benson, C. A. Bischoff, J. Borrill, V. Buza, E. Calabrese, R. Caldwell, J. E. Carlstrom, C. L. Chang, T. M. Crawford, F.-Y. Cyr-Racine, F. De Bernardis, T. de Haan, S. di Serego Alighieri, J. Dunkley, C. Dvorkin, J. Errard, G. Fabbian, S. Feeney, S. Ferraro, J. P. Filippini, R. Flauger, G. M. Fuller, V. Gluscevic, D. Green, D. Grin, E. Grohs, J. W. Henning, J. C. Hill, R. Hlozek, G. Holder, W. Holzapfel, W. Hu, K. M. Huffenberger, R. Keskitalo, L. Knox, A. Kosowsky, J. Kovac, E. D. Kovetz, C.-L. Kuo, A. Kusaka, M. Le Jeune, A. T. Lee, M. Lilley, M. Loverde, M. S. Madhavacheril, A. Mantz, D. J. E. Marsh, J. McMahon, P. D. Meerburg, J. Meyers, A. D. Miller, J. B. Munoz, H. N. Nguyen, M. D. Niemack, M. Peloso, J. Peloton, L. Pogosian, C. Pryke, M. Raveri, C. L. Reichardt, G. Rocha, A. Rotti, E. Schaan, M. M. Schmittfull, D. Scott, N. Sehgal, S. Shandera, B. D. Sherwin, T. L. Smith, L. Sorbo, G. D. Starkman, K. T. Story, A. van Engelen, J. D. Vieira, S. Watson, N. Whitehorn, and W. L. Kimmy Wu, CMB-S4 Science Book, First Edition, ArXiv e-prints (2016), arXiv:1610.02743.
- [8] P. Ade, J. Aguirre, Z. Ahmed, S. Aiola, A. Ali, D. Alonso, M. A. Alvarez, K. Arnold, P. Ashton, J. Austermann, and et al., The Simons Observatory: science goals and forecasts, *JCAP* **2019**, 056 (2019), arXiv:1808.07445 [astro-ph.CO].
- [9] B. Keating, S. Moyerman, D. Boettger, J. Edwards, G. Fuller, F. Matsuda, N. Miller, H. Paar, G. Rebeiz, I. Schanning, M. Shimon, N. Stebor, K. Arnold, D. Flanagan, W. Holzapfel, J. Howard, L. Kermish, A. Lee, M. Lungu, M. Myers, H. Nishino, R. O'Brient, E. Quealy, C. Reichardt, P. Richards, C. Shimmmin, B. Steinbach, A. Suzuki, O. Zahn, J. Borrill, C. Cantalupo, E. Kisner, E. Linder, M. Sholl, H. Spieler, A. Anthony, N. Halverson, J. Errard, G. Fabbian, M. Le Jeune, R. Stompor, A. Jaffe, D. O'Dea, Y. Chinone, M. Hasegawa, M. Hazumi, T. Matsumura, H. Morii, A. Shimizu, T. Tomaru, P. Hyland, M. Dobbs, P. Ade, W. Grainger, and C. Tucker, Ultra High Energy Cosmology with POLARBEAR, ArXiv e-prints (2011), arXiv:1110.2101 [astro-ph.CO].
- [10] H. Li, S.-Y. Li, Y. Liu, Y.-P. Li, Y. Cai, M. Li, G.-B. Zhao, C.-Z. Liu, Z.-W. Li, H. Xu, D. Wu, Y.-J. Zhang, Z.-H. Fan, Y.-Q. Yao, C.-L. Kuo, F.-J. Lu, and X. Zhang, Probing primordial gravitational waves: Ali CMB Polarization Telescope, *National Science Review* **6**, 145 (2018), <http://oup.prod.sis.lan/nsr/article-pdf/6/1/145/27981397/nwy019.pdf>.
- [11] H. Liu, J. Creswell, and P. Naselsky, E and B families of the Stokes parameters in the polarized synchrotron and thermal dust foregrounds, *JCAP* **5**, 059 (2018), arXiv:1804.10382.
- [12] A. Rotti and K. Huffenberger, Real-space computation of E/B-mode maps. Part I. Formalism, compact kernels, and polarized filaments, *JCAP* **2019**, 045 (2019), arXiv:1807.11940 [astro-ph.CO].
- [13] M. Zaldarriaga and U. c. v. Seljak, All-sky analysis of polarization in the microwave background, *Phys. Rev. D* **55**, 1830 (1997).
- [14] W. Hu and M. White, CMB anisotropies: Total angular momentum method, *Phys. Rev. D* **56**, 596 (1997), arXiv:astro-ph/9702170 [astro-ph].
- [15] K. M. Górski, E. Hivon, A. J. Banday, B. D. Wandelt, F. K. Hansen, M. Reinecke, and M. Bartelmann, HEALPix: A Framework for High-Resolution Discretization and Fast Analysis of Data Distributed on the Sphere, *Astrophys. J.* **622**, 759 (2005), astro-ph/0409513.
- [16] N. R. Walborn, I. D. Howarth, D. J. Lennon, P. Massey, M. S. Oey, A. F. J. Moffat, G. Skalkowski, N. I. Morrell, L. Drissen, and J. W. Parker, A New Spectral Classification System for the Earliest O Stars: Definition of Type O2, *Astr. J.* **123**, 2754 (2002).
- [17] J. E. Gaustad, P. R. McCullough, W. Rosing, and D. Van Buren, A Robotic Wide-Angle H α Survey of the Southern Sky, *Publications of the Astronomical Society of the Pacific* **113**, 1326 (2001), arXiv:astro-ph/0108518 [astro-ph].
- [18] E. Bica, C. Bonatto, C. M. Dutra, and J. F. C. Santos, A general catalogue of extended objects in the Magellanic System, *Mon. Not. R. Astr. Soc.* **389**, 678 (2008), arXiv:0806.3049 [astro-ph].
- [19] H. Liu, Fingerprint of Galactic Loop I on polarized microwave foregrounds, *Astr. Astrophys.* **617**, A90 (2018), arXiv:1806.06532.
- [20] R. P. Norris, J. D. Collier, R. M. Crocker, I. Heywood, P. Macgregor, L. Rudnick, S. Shabala, H. Andernach, E. da Cunha, J. English, M. Filipovic, B. S. Koribalski, K. Luken, A. Robotham, S. Sekhar, J. E. Thorne, and T. Vernstrom, MeerKAT uncovers the physics of an Odd Radio Circle, arXiv e-prints , arXiv:2203.10669 (2022), arXiv:2203.10669 [astro-ph.GA].
- [21] M. Zaldarriaga, Nature of the E-B decomposition of CMB polarization, *Phys. Rev. D* **64**, 103001 (2001), astro-ph/0106174.
- [22] Z. Fuzhen, Quaternions and matrices of quaternions, *Linear Algebra and its Applications* **251**, 21 (1997).